Geoacoustic Inversion Using Backpropagation

Cheolsoo Park, Woojae Seong, *Member, IEEE*, Peter Gerstoft, and William S. Hodgkiss, *Member, IEEE*

***Abstract*—This paper presents inversion results of the 2006 Shallow Water Experiment (SW06) data measured on a vertical line array. A low-frequency (100–900 Hz) chirp source was towed along two tracks (circle, straight line) at 30-m depth. For the inversions, a three-step optimization scheme is applied to the data using very fast simulated reannealing (VFSR). The objective function is defined by the energy of the backpropagated signal from the array to the source. At each step, water-column sound-speed profile (SSP), experimental geometry, and geoacoustic parameters are inverted successively. An environmental model is employed consisting of a linear segmented SSP in the water column, a sediment layer, and a half-space. The geometric parameter inversion results show good agreement with *in situ* measurements. Finally, the estimated geoacoustic parameters show that the experimental site near the vertical line array (VLA) is fairly homogeneous in bottom properties consisting of a 21-m-thick sediment layer with sound speed of around 1600 m/s over a hard basement whose sound speed is approximately 1750 m/s.**

***Index Terms*—2006 Shallow Water Experiment, backpropagation, geoacoustic inversion, multistep optimization, time-domain inversion, very fast simulated reannealing (VFSR).**

I. Introduction

GEOACOUSTIC inversion is a useful tool for estimating not only seabed properties but also other information such as source position, bathymetry, and sound-speed profile (SSP) of the water column. The seabed properties are especially important in shallow water since sound propagation is strongly influenced by the bottom. Therefore, various methods for estimating the geoacoustic parameters of the ocean bottom via remote sensing have been developed.

This paper is focused on the broadband time-domain inversion of nearfield (<600 m) acoustic data. Most geoacoustic inversions have been performed in the frequency domain using either narrowband or broadband data [1], [2]. However, the time-domain approach has received attention as well [3]–[9]. When arrivals of different eigenrays are resolved, geoacoustic parameters can be inverted using travel times and/or amplitudes of measured and simulated data [6], [9]. Otherwise, full waveform matching seeking the best correlation value between the measured and replica time series has been used [4], [7]. The model-based matched filter has also been useful for time-domain inversion [3], [5]. Especially for the nearfield broadband data, a set of time-domain signals shows a typical structure of multiple arrivals such as direct, bottom-, and surface-reflected waves depending on experimental setups and environments. To exploit the arrival structure directly in the inversion, a time-domain approach is used in this paper.

It has been demonstrated that the sound wave received by a hydrophone, time reversed, and retransmitted from the receiver position will focus at the source position [11]. This also has been explained as a matched filter [10], or generalized beamformer [12]. Numerically, equivalent processing can be implemented by backpropagating the time-reversed signal. Then, the energy of the backpropagated signal becomes a measure of environmental mismatch, which can be used in source localization [12] and geoacoustic inversion [8].

A set of experiments [2006 Shallow Water Experiment (SW06)] was carried out in shallow water near the New Jersey shelf break in summer 2006 [13]. One objective of SW06 was the acoustic characterization of the ocean bottom using sources, covering various bands of frequency. This paper presents the inversion results from the low-frequency chirp data (100–900 Hz) recorded by a vertical line array (VLA) while the source was following circular and straight paths at ranges 200–600 m. The inversion approach is based on the method described in [8] that was applied to ship noise recorded on a horizontal towed array. The objective function used in the inversion is defined using the energy of the backpropagated signals from the array to the source. Then, a three-step optimization is applied to the objective function to find the optimum environmental parameters.

The paper is organized as follows. In Section II, we describe the experiments and the acoustic data. In Section III, the inversion scheme is presented including the derivation of the objective function. Section III presents inversion results for the two track events and Section IV summarizes the paper.

II. Description Of Experiments

A. The Experiments

The experimental data was collected near the New Jersey continental shelf break [13]. The acoustic data were recorded on a VLA located at (39° 1.477′ N, 73° 2.259′ W) as shown in

Manuscript received April 21, 2009; manuscript revised November 09, 2009. Date of manuscript acceptance December 22, 2009; date of publication March 29, 2010; date of current version November 30, 2010. This work was supported by the U.S. Office of Naval Research under Grant N00014-05-1-0264, the Korea Research Foundation under Grant KRF-2009-013-D00139, and KORDI Grant PES132B.

Associate Editor: J. F. Lynch.

C. Park was with the Marine Physical Laboratory, Scripps Institution of Oceanography, University of California San Diego (UCSD), La Jolla, CA 92093 USA. He is now with the Maritime and Ocean Engineering Research Institute (MOERI)/Korean Ocean Research and Development Institute (KORDI), Daejeon 305-343, Korea (e-mail: parkcs@moeri.re.kr).

W. Seong is with the Marine Physical Laboratory, Scripps Institution of Oceanography, University of California San Diego (UCSD), La Jolla, CA 92093 USA, on leave from the Research Institute of Marine Systems Engineering, Seoul National University, Seoul 151-744, Korea (e-mail: wseong@snu.ac.kr).

P. Gerstoft and W. S. Hodgkiss are with the Marine Physical Laboratory, Scripps Institution of Oceanography, University of California San Diego (UCSD), La Jolla, CA 92093 USA (e-mail: gerstoft@ucsd.edu; whodgkiss@ucsd.edu).

Color versions of one or more of the figures in this paper are available online at http://ieeexplore.ieee.org.

Digital Object Identifier 10.1109/JOE.2010.2040659

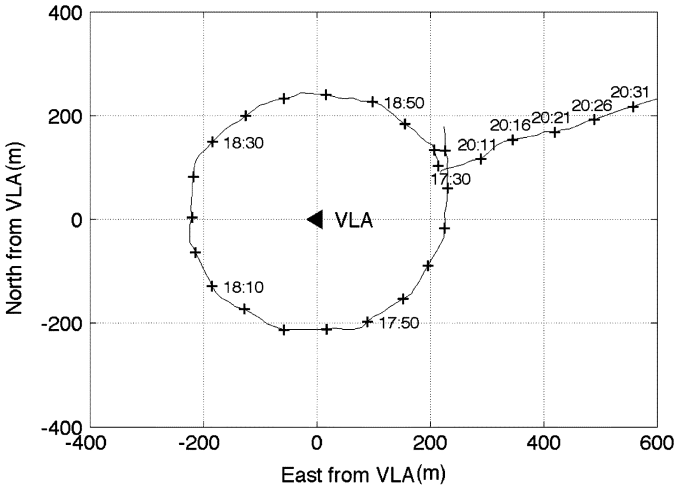

Fig. 1. Experimental configuration. Circular and straight paths with respect to the VLA are shown. The tick interval is 5 min.

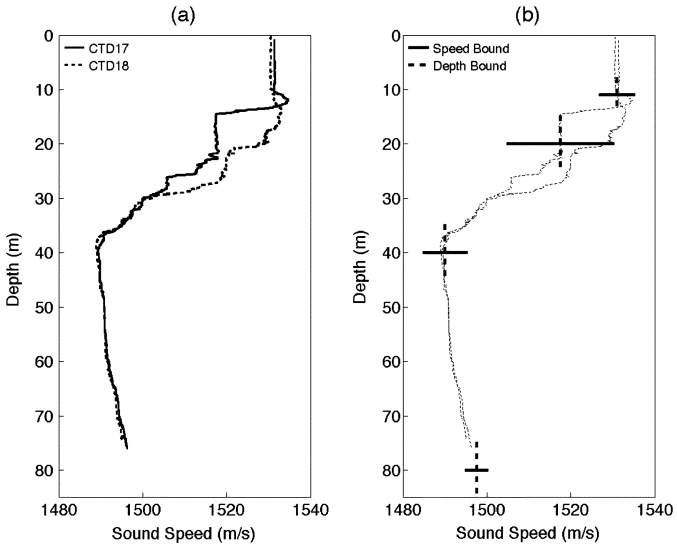

Fig. 2. SSPs (a) derived from CTD17 (19:17:00 UTC) and CTD18 (19:54:00 UTC). The water-column SSP is modeled as a four-segment linear SSP for the inversion and the search bounds for the sound speeds and break points of each segment are shown in (b).

Fig. 1. The VLA had 16 hydrophones with 3.75-m spacing. The bottom hydrophone (channel 1) was 8.2 m above the seafloor. The seabed constitutes of low-speed clay over the so-called "R"-reflector that is approximately 20 m below the seafloor [13]–[18].

During the experiment, the source was towed by the *R/V Knorr* at 0.5–1 kn on the two tracks shown in Fig. 1. The first track was a circle around the VLA with a nominal radius of 230 m. The second was a straight run. During both tracks, the source was at 30-m depth and emitting continuously a 1-s linear frequency modulation (LFM) transmission swept from 100 to 900 Hz. The bathymetry along the tracks was almost flat with a water depth of roughly 79 m.

The circle event started at 17:25:00 coordinated universal time (UTC) on August 27, 2006 and finished at 19:00:00 UTC. The straight event was carried out from 20:07:00 to 21:30:00 UTC. Two conductivity–temperature–depths (CTDs), CTD17 (19:17:00 UTC) and CTD18 (19:54:00 UTC), were obtained

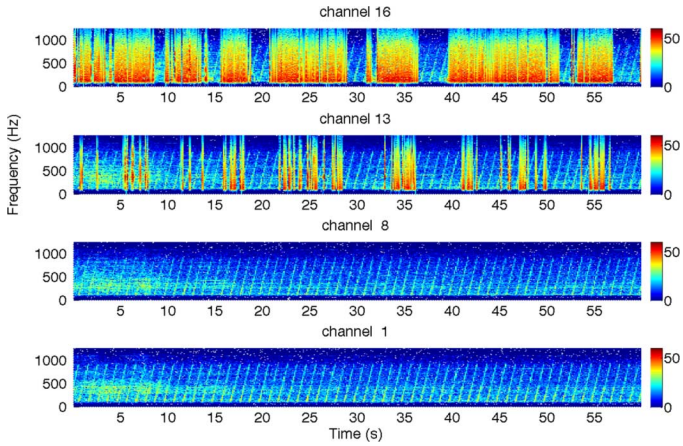

Fig. 3. Spectrograms of channels 1, 8, 13, and 16 of acoustic data measured at 20:16:00 UTC.

near VLA1 during this period. Fig. 2(a) shows the water-column SSPs derived from the two CTDs. Significant differences between two SSPs are observed between depths of 10 and 30 m where fluctuations in the thermocline region are found.

B. Acoustic Data Processing

The raw data obtained from 16 hydrophones on the VLA were matched filtered using a synthetic 1-s 100–900-Hz LFM waveform. The sampling rate was reduced to 10 kHz (downsampled from 50 kHz). The resulting compressed matched-filtered data are used for the inversions.

Spectrograms of acoustic data at 20:16:00 UTC, containing 60 transmissions, are shown in Fig. 3. Broadband noise likely from large ocean swell due to tropical storm Ernesto is observed in the spectrograms. This is a persistent feature for all acoustic data. Disturbances are strongest at the hydrophone (channel 16) nearest to the sea surface. For the inversion, the least corrupted 1-s transmission for each 1-min data was chosen by visual inspections.

III. Inversion Approach

A. Objective Function Using Backpropagation

In an ideal linear time invariant system without noise, the propagation of a source signal $s(t)$, e.g., a chirp signal [7] or ship noise [8], from a source $\mathbf{r}_s$ to a receiver $\mathbf{r}_r$ through a medium described by the parameter vector $\mathbf{m}_0$, is given by the convolution with the medium impulse response $h(t)$ as

$$d(t, \mathbf{r}_s, \mathbf{r}_r, \mathbf{m}_0) = s(t) * h(t, \mathbf{r}_s, \mathbf{r}_r, \mathbf{m}_0) \tag{1}$$

where $d(t, \mathbf{r}_s, \mathbf{r}_r, \mathbf{m}_0)$ is the signal received by a hydrophone and $*$ is the convolution operator. If the received signal is time reversed and propagated from the receiver to the source position, the backpropagated signal becomes

$$\begin{aligned} &b(t, \mathbf{r}_r, \mathbf{r}_s, \mathbf{m}_0) \\ &\quad = d(T-t, \mathbf{r}_s, \mathbf{r}_r, \mathbf{m}_0) * h(t, \mathbf{r}_r, \mathbf{r}_s, \mathbf{m}_0) \\ &\quad = s(T-t) * (h(T-t, \mathbf{r}_s, \mathbf{r}_r, \mathbf{m}_0) * h(t, \mathbf{r}_r, \mathbf{r}_s, \mathbf{m}_0)) \end{aligned} \tag{2}$$

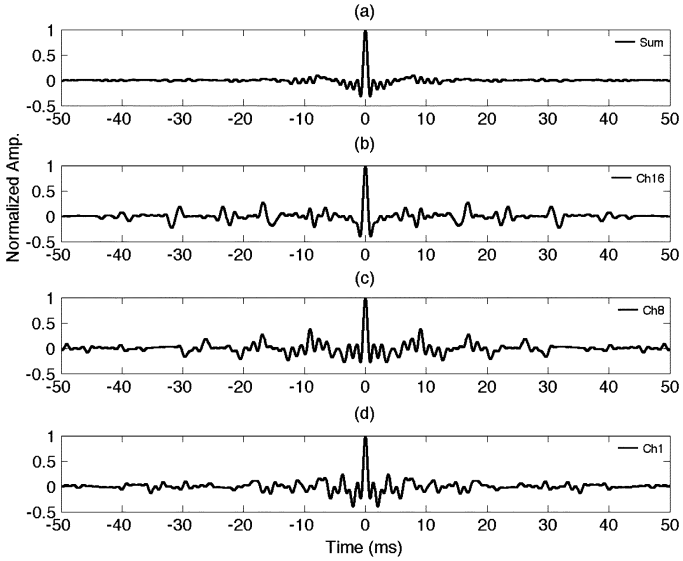

Fig. 4. Autocorrelation of the impulse responses: (a) sum of all 16 hydrophones, (b) channel 16, (c) channel 8, and (d) channel 1.

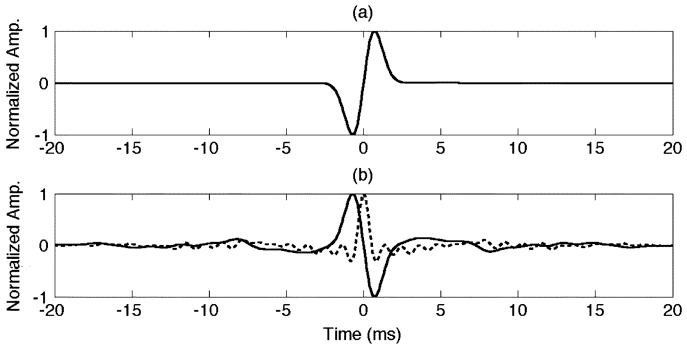

Fig. 5. (a) Source waveform and (b) backpropagated signal at the source position (solid) along with the sum of the autocorrelations of impulse responses (dashed).

where T is a maximum time extent of the received signal. Since the source and receiver position can be exchanged, the $h(T-t,\mathbf{r}_s,\mathbf{r}_r,\mathbf{m}_0)*h(t,\mathbf{r}_r,\mathbf{r}_s,\mathbf{m}_0)$ in (2) is a time-delayed autocorrelation of the impulse response $h(t,\mathbf{r}_s,\mathbf{r}_r,\mathbf{m}_0)$. Therefore, the backpropagated signal is equivalent to the convolution between the time-reversed source waveform and the autocorrelation of the medium impulse response.

Figs. 4 and 5 show simulations of the backpropagation for an 80-m-deep Pekeris waveguide. The sound speeds of the water column and the bottom are 1500 and 1600 m/s, respectively. The bottom density is 1.8 10^3 kg/m^3. The 100–900-Hz LFM source is located at 30-m depth and 230-m range from the VLA. Fig. 4(b), (c), and (d) shows the autocorrelation of the impulse responses for channels 1, 8, and 16, respectively. Fig. 4(a) is the sum of autocorrelations for all 16 channels. It can be seen from Fig. 4(b), (c), and (d) that the autocorrelation for an individual channel contains a mainlobe and multiple sidelobes. If the autocorrelations for different channels are added coherently in time, the mainlobe will be reinforced whereas the sidelobes are canceled by destructive interference. As a result, the mainlobe becomes dominant and approaches the bandlimited impulse response of free space when the number of channels is large as shown in Fig. 4(a).

A characteristic of time-reversed backpropagation from multiple hydrophones is that the measured signal resembles the time-reversed source waveform as is seen in (2). The source waveform in (1) and (2) is arbitrary and a first derivative Gaussian waveform, which is widely used for modeling of seismic wave propagation [19], [20], is chosen to illustrate this characteristic. The first derivative Gaussian waveform $(t-t_0)\exp(-\omega^2(t-t_0)^2)$ is shown in Fig. 5(a). The source signal is bandpass filtered over 100–900 Hz. The waveform of the sum of backpropagated signals for all channels is shown (solid) in Fig. 5(b). The autocorrelation of the impulse response [Fig. 4(a)] is also shown (dashed) as a reference. It is evident that the resulting backpropagated waveform becomes similar to the time-reversed source waveform since the sum of impulse response autocorrelations approaches that of the bandlimited impulse response of free space. In Figs. 4 and 5, each signal is plotted after normalizing for its maximum to be 1 although maximum amplitudes might be different from each other. As for the backpropagated signals, quantitative discussion for the Pekeris waveguide example is given after (3).

For geoacoustic inversion, a replica can be substituted for the true impulse response. When the environment for the replica is the same as the true environment, the backpropagated signal will focus spatially at the original source position with the waveform being approximately equal to the time-reversed source signal.

Inversion parameters describing the environment (including source/receiver parameters) are represented by the replica model vector $\mathbf{m} = [m_1, m_2, \ldots, m_{N_m}]^T$ where $[]^T$ is the transpose operator and N_m is the number of parameters. The normalized backpropagated signal is defined as [8]

$$b_n(t,\mathbf{m}) = \frac{1}{N_r}\sum_{k=1}^{N_r} \frac{d_k(T-t)}{\sqrt{\int_0^T |d_k(\tau)|^2 d\tau}} * \frac{h_k(t,\mathbf{m})}{\sqrt{\int_0^T |h_k(\tau,\mathbf{m})|^2 d\tau}} \tag{3}$$

where $d_k(t)$ and $h_k(t,\mathbf{m})$ are the measured signal and replica for the kth hydrophone of the N_r element array, and T is the maximum time extent of the signals. The defined backpropagated signal corresponds to the average of normalized cross-correlation functions for all channels. The purpose of the normalization of each channel in (3) is to remove the dependency on source and replica energy in the cross correlation. As for the Pekeris waveguide simulation (Figs. 4 and 5), the normalized cross-correlation peaks at the selected channels 1, 8, and 16 are 0.63, 0.61, and 0.68, respectively. As a result of averaging for all 16 channels, the maximum of the normalized backpropagated signal becomes 0.614, which is smaller than the peak of the normalized autocorrelation function 1 due to the effect of source waveform [see (2)].

If the data $d_k(t)$ are the impulse response measured [3] or estimated [5], maximizing (3) over the whole time lag t becomes similar to the objective function employed in time-series matching inversions [3]–[5], [7]. Here, the objective function to be maximized for the inversion is defined as

$$\phi(\mathbf{m}) = \max_{t_1}\left[\int_{t_1}^{t_1+\Delta t} |b_n(t,\mathbf{m})|^2 dt\right], \quad \text{for } 0 \le t_1 \le T-\Delta t. \tag{4}$$

The Δt is a focal time width of the backpropagated signal and depends on the source waveform such that most energy of the source is confined within Δt [8], [12]; see Section IV. The spatial resolution of time reversal is described in [21].

An influential factor in the correlation of signals is time delay. Mismatches in time delays result in a considerable reduction of correlation, but the signal amplitudes have less effect. Therefore, the objective function is more sensitive to inversion parameters influencing the time delay such as source/receiver positions, water depth, layer thickness, and sound speed than those mostly influencing the amplitude such as densities and attenuations.

B. Inversion Scheme

The raw acoustic data at a hydrophone of the VLA, ignoring noise, are

$$r(t) = s_0(t) * h(t) \tag{5}$$

where $s_0(t)$ is a 1-s LFM (100–900 Hz) signal. The matched-filtered signal becomes

$$\begin{aligned} d(t) &= s_0(-t) * r(t) = (s_0(-t) * s_0(t)) * h(t) \\ &= s(t) * h(t) \end{aligned} \tag{6}$$

where $s(t)$ is now the compressed wavelet of the LFM signal, which is equivalent to (1). In the following, the acoustic data refer to the matched-filtered signal in (6).

Inversion parameters are categorized into three groups: geometric, geoacoustic, and SSP groups. The geometric group includes the source depth, source range, tilt of the VLA, and water depth. The geoacoustic group consists of the parameters describing the bottom such as sound speed, density, and layer thickness. Based on the model for the experimental site near the VLA [9], [18], [22], a range-independent model with a sediment layer over a half-space is adopted. Therefore, the geoacoustic parameters are sound speeds and densities of the sediment layer and the half-space and the sediment layer thickness. The sediment layer and the bottom are assumed isospeed. Attenuation is excluded due to low sensitivity to attenuation at short ranges.

The water-column SSP shows significant variability both in time and space. Also, the CTD measurements were not preformed simultaneously with the acoustic measurements. The measured SSP in Fig. 2(a) is composed of three subregions: upper constant region, thermocline region with multiple gradients, and lower isogradient region. Here, the water column is divided into four segments: one for upper isospeed region, two for thermocline, and one for lower isogradient region. The sound speed is modeled as a linear profile in each segment and discontinuity is not allowed at the segment break points. The search bounds for the break points are shown in Fig. 2(b).

The inversion is performed via an optimization process that searches the parameters to maximize the objective function $\phi(\mathbf{m})$ in (4). Direct and surface-reflected signals usually have large amplitudes. However, they contain mostly the geometric and the ocean SSP information and thus do not contribute directly to the inversion of bottom properties. If all the parameters are inverted simultaneously, the geometric parameters or the SSP parameters dominate over the geoacoustic parameters in the search process. To prevent this, it is desired that the parameters be inverted separately based on their relative sensitivities. The multistep inversion also reduces the number of parameters in each step permitting an efficient optimization [23].

A three-step approach is applied to the inversion as follows.

1) The target parameters are the SSP group. At first, the inversion is carried out using a simple half-space model whose parameters are the SSP group, the geometric group, and the sound speed of the bottom. Since bottom density is not important, it is fixed at 2 10^3 kg/m^3. Although the final bottom model is a sediment layer over a half-space, the simple half-space model used in the first step is chosen for efficiency. Among all the inverted parameters, only the SSP parameters are passed to the next inversions.
2) The target parameters are the geometric group. The inversion still is carried out using the simple half-space model. The inversion parameters are the geometric and geoacoustic parameters. The inverted geometric parameters along with the SSP parameters are passed to the final inversion.
3) The final inversion is carried out for the geoacoustic parameters using the sediment layer over a half-space bottom model.

In all inversions, the very fast simulated reannealing (VFSR [24]) global search algorithm is used. This is a modified version of simulated annealing (SA) and has been useful in geophysical and geoacoustic applications [7], [25]. It consists of successive quenching sequences where the quenching temperature is lowered according to a predetermined schedule. We applied 50 successive quenching sequences to the first and second steps and 100 quenching sequences to the third step of the inversion. For each sequence, 50 parameter evaluations are carried out. Therefore, 10000 replica calculations are performed for the entire inversion.

For the forward model, a ray-based time-domain modeling method is used; see the Appendix.

IV. Inversion Results

The signal truncation time T in (3) is chosen as 1 s so that all the arrivals are included within it. Most of the energy of the matched-filtered 100–900-Hz chirp was concentrated in the mainlobe of 2-ms width. Therefore, the focal time width Δt in (4) is set to 2 ms. Note that a single ping was used for each inversion. It is expected that the acoustic data will show temporal variations due to environmental effects such as SSP fluctuation and surface wave activity.

A. Backpropagation and Parameter Sensitivity

To understand the characteristics of backpropagation of the received signals, we simulated the backpropagated signals from the VLA to candidate source positions using the inverted environment for the data at 20:12:00 UTC. Fig. 6(a) and (b) shows the envelopes of the backpropagated array data [$b_n(t, \mathbf{m})$ in (3)] as a function of depth and range, while the other parameters are those obtained in the inversion. The inverted source range is 302 m and depth is 28.5 m. The amplitudes are normalized to a maximum of 1. Since the acoustic data are compressed as in (6), the backpropagated signal is also compressed. From the figure, a

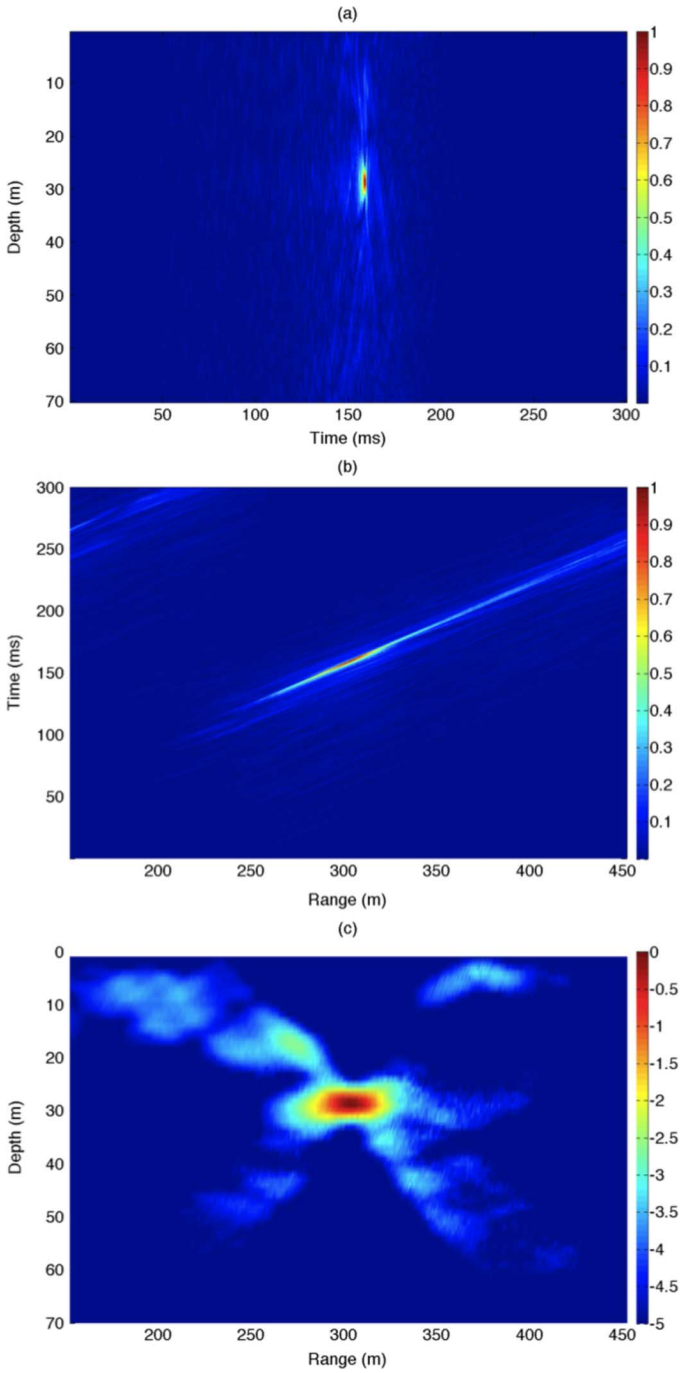

Fig. 6. Envelopes of back propagated array data in (3) with varying (a) depth and (b) range. (c) Ambiguity surface of the objective function in (4) (dB) using $\Delta t = 2$ ms.

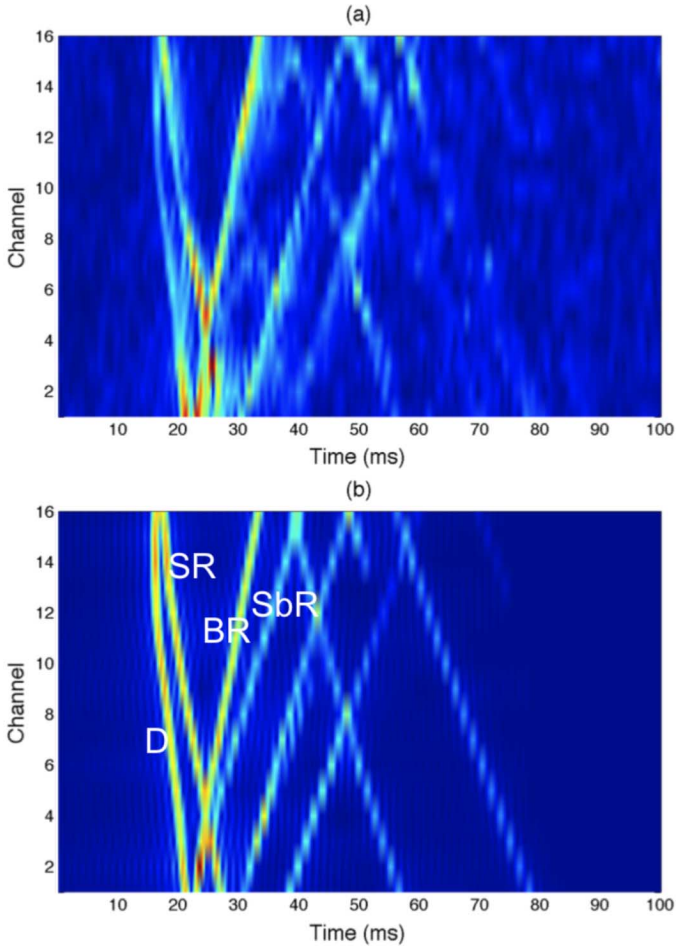

Fig. 7. Envelopes of (a) matched-filtered array data at 20:12:00 UTC and (b) impulse response simulated using inversion results (D: direct arrivals, SR: surface reflected arrivals, BR: bottom reflected arrivals, SbR: sub-bottom reflected arrivals).

strong mainlobe with minor sidelobes is observed around the inverted source position. The focusing of the signal is mainly due to the constructive interference and spatial coherence of the autocorrelations. The ambiguity surface in Fig. 6(c) [$\phi(\mathbf{m})$ in (4)] shows a good focus of the backpropagated array data at the correct source position. The matched-filtered array data at 20:12:00 UTC and the simulated impulse response using the inverted parameters are shown in Fig. 7.

A set of geometric and geoacoustic parameter inversion results for the data at 20:12:00 UTC is presented as scatter plots in Fig. 8. The scatter plots represent the relative power (in decibels) of the objective function (y-axis) for the corresponding parameter (x-axis) evaluated during optimization. The scatter plots give information on the behavior of parameters such as sensitivity and coupling [8]. If the objective function is sensitive to a parameter, it decreases rapidly from the maximum.

The geometric parameters commonly show high sensitivities to the objective function. Among the geoacoustic parameters, the sediment layer parameters are more sensitive than the half-space parameters. There are distinct maxima both in layer sound speed and in thickness of the layer of around 1600 m/s and 21 m, respectively.

B. Circle Event

This section presents the results of the inversions for the circle event. The circle event was carried out for 1.5 h from 17:25:00 to 19:00:00 UTC; see Fig. 1. Twenty 1-s-long records of acoustic data at 5-min intervals are inverted.

Fig. 9 shows the inverted parameters. The search bounds span the y-axis range for each parameter except for the SSP described in Section III-B [see Fig. 2(b)]. During the event, some geometrical parameters such as source range, source depth, and water depth were measured *in situ* with nominal values 230, 30, and 79 m, respectively. These values agree well with the inversion

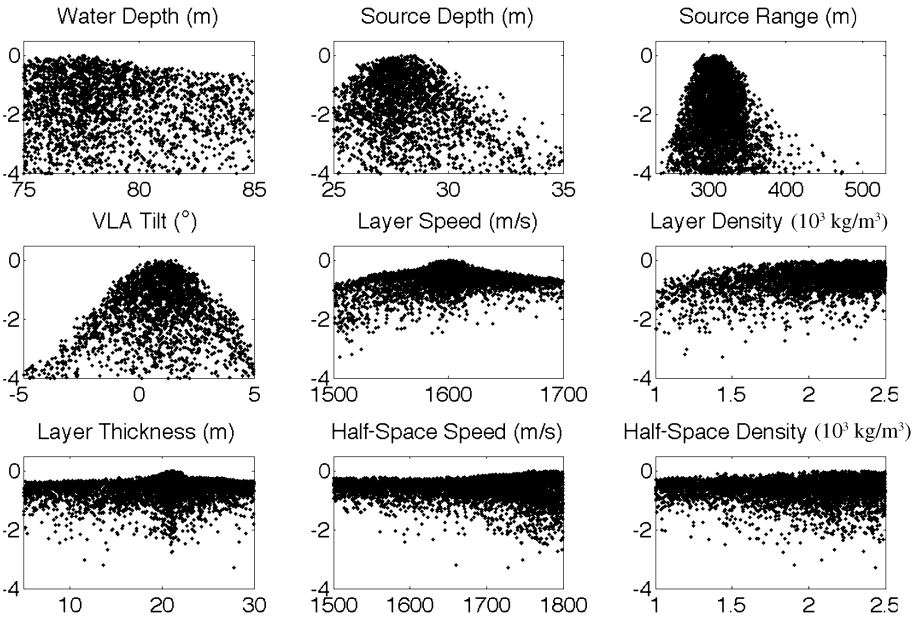

Fig. 8. Scatter plots of the VFSR search for array data at 20:12:00 UTC. The y-axis of the plot is relative power (in decibels) of the objective function evaluated during the optimization and the x-axis spans the parameter search bound.

TABLE I
INVERTED GEOACOUSTIC PARAMETERS FOR THE CIRCLE AND STRAIGHT EVENTS

CASE	Layer			Half-Space	
	Speed (m/s)	Density (10^3 kg/m^3)	Thickness (m)	Speed (m/s)	Density (10^3 kg/m^3)
Circle	1606 ± 9	1.9 ± 0.1	21.2 ±0.8	1740 ±30	2.2 ±0.3
Straight	1601 ± 6	2.3 ± 0.2	21.3 ±0.9	1761 ±29	2.3 ±0.2

results. The source range estimated from the ship differential global positioning system (DGPS) is compared with the inverted range on the plot. The inverted tilt angle shows a periodic pattern, as expected for the circle. According to the tilt meter on the VLA, the tilt angle was 1.8°± 1° during the circle event. The absolute value of the peak inverted tilt angles is within the range of the measured tilts.

The inversion results for the geoacoustic parameters support the conclusion that the seabed around the site consists of a low-speed layer over a high-speed reflector. The experimental site even appears to be homogeneous in terms of the bottom properties with the inverted sound speeds of the bottom and layer thicknesses showing little variability for the sampled data. The statistics (mean ± standard deviation) for the geoacoustic parameter estimates from 20 samples of acoustic data are given in Table I. The seabed around the VLA appears to be homogeneous and is composed of a 21.2-m-thick layer sediment with sound speed 1606 m/s over the so-called "R"-reflector with sound speed 1740 m/s.

The inverted sound speeds of the water column show large fluctuations especially in the thermocline. For the SSP inversion, an alternative would be to use an empirical orthogonal function (EOF) model [9], [22], [26].

The normalized powers (in decibels) of the maximum objective function values obtained at all three steps of each inversion are given in the lower middle panel of Fig. 9. The powers become higher as the inversion step advances, which is expected with the multistep inversion. From the objective function values of inversion steps 2 and 3, the contribution of the reflection from the "R"-reflector to the objective function can be quantified. This corresponds to the difference of the objective function values from inversion steps 2 and 3. The contribution is around 0.2 dB more than the normalized backpropagated energy evaluated without the sub-bottom arrivals as shown in the objective function plots of Figs. 9 and 10 of the straight event.

C. Straight Event

This section presents the results of the inversions during the straight event from 20:11:00 to 20:30:00 UTC; see Fig. 1. Twenty 1-s-long records of acoustic data at 1-min intervals from 21:11:00 UTC are inverted.

Fig. 10 shows the inverted parameters for the straight event. The search bounds are the same as for the circle event except for the source range. The search bounds of the range are 380±150 m for the first half of the data and 530±150 m for the rest. The nominal source depth is 30 m and water depth is 79 m. The inverted and nominal values for the geometrical parameters match well. As a reference, the range of the source obtained from the onboard DGPS is also given in the inverted source range plot. Comparing two data validates the inversion results. The tilt angle measured from 20:11:00 to 20:30:00 UTC was 1.6°±1°. The projected tilt onto the vertical plane of the ship trajectory corresponds to 1.5° and agrees with the inverted angle.

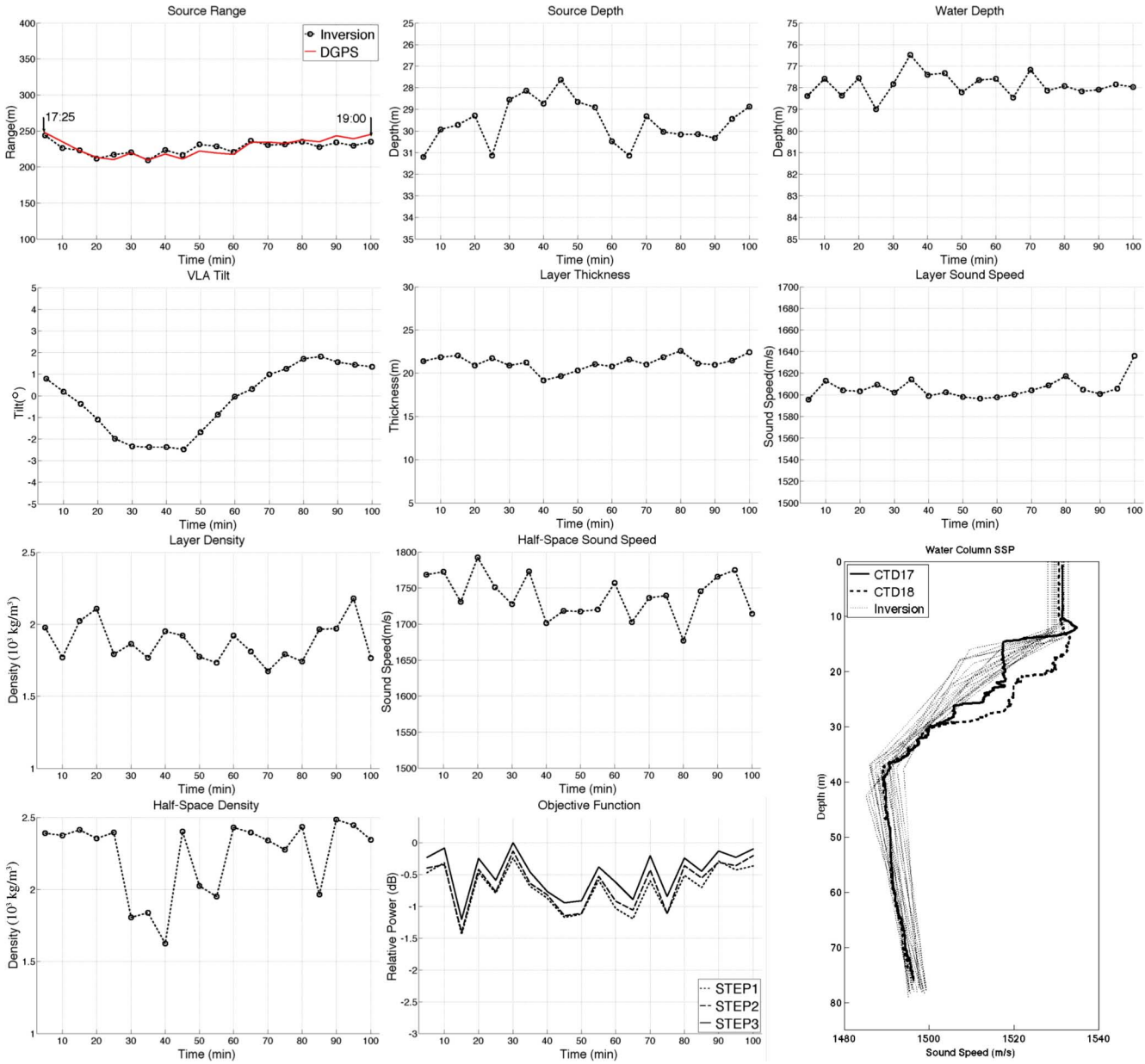

Fig. 9. Inversion results from the circle event (17:25:00 to 19:00:00 UTC). In the plot of source range, the range estimated from the ship DGPS is compared with the inverted range.

The inversion results for the geoacoustic parameters of the straight event also support the conclusion that the seabed around the array site consists of a low-speed sediment layer over a high-speed reflector. The statistics (mean±standard deviation) for the geoacoustic parameter estimates from 20 samples of acoustic data also are given in Table I. The seabed structure along the straight track appears to be homogeneous and is composed of the 21.3-m-thick sediment layer with sound speed 1601 m/s over the so-called "R"-reflector with sound speed 1761 m/s.

V. Conclusion

Time-domain geoacoustic inversion results for the SW06 experimental data (100–900 Hz chirps) are presented for nearfield measurements with a source range less than 600 m. For the inversion, the objective function was defined as the energy of backpropagated acoustic array data from the VLA to the source. A three-step inversion scheme was applied to the data and the VFSR algorithm was used as an optimizer for the objective function.

The inversion results from the circle event showed that the geoacoustic properties around the VLA appear to be homogeneous and the bottom is composed of a 21.2-m-thick sediment layer with low sound speed (1606 m/s) over the faster "R"-reflector (1740 m/s). The inversion results form the straight run also yielded similar results estimating a 21.3-m sediment layer (1601-m/s sound speed) and faster sub-bottom (1761-m/s sound speed).

Appendix

A. The Forward Model

A ray-based forward model is used to simulate waveforms in the time domain and it is implemented as follows. The acoustic

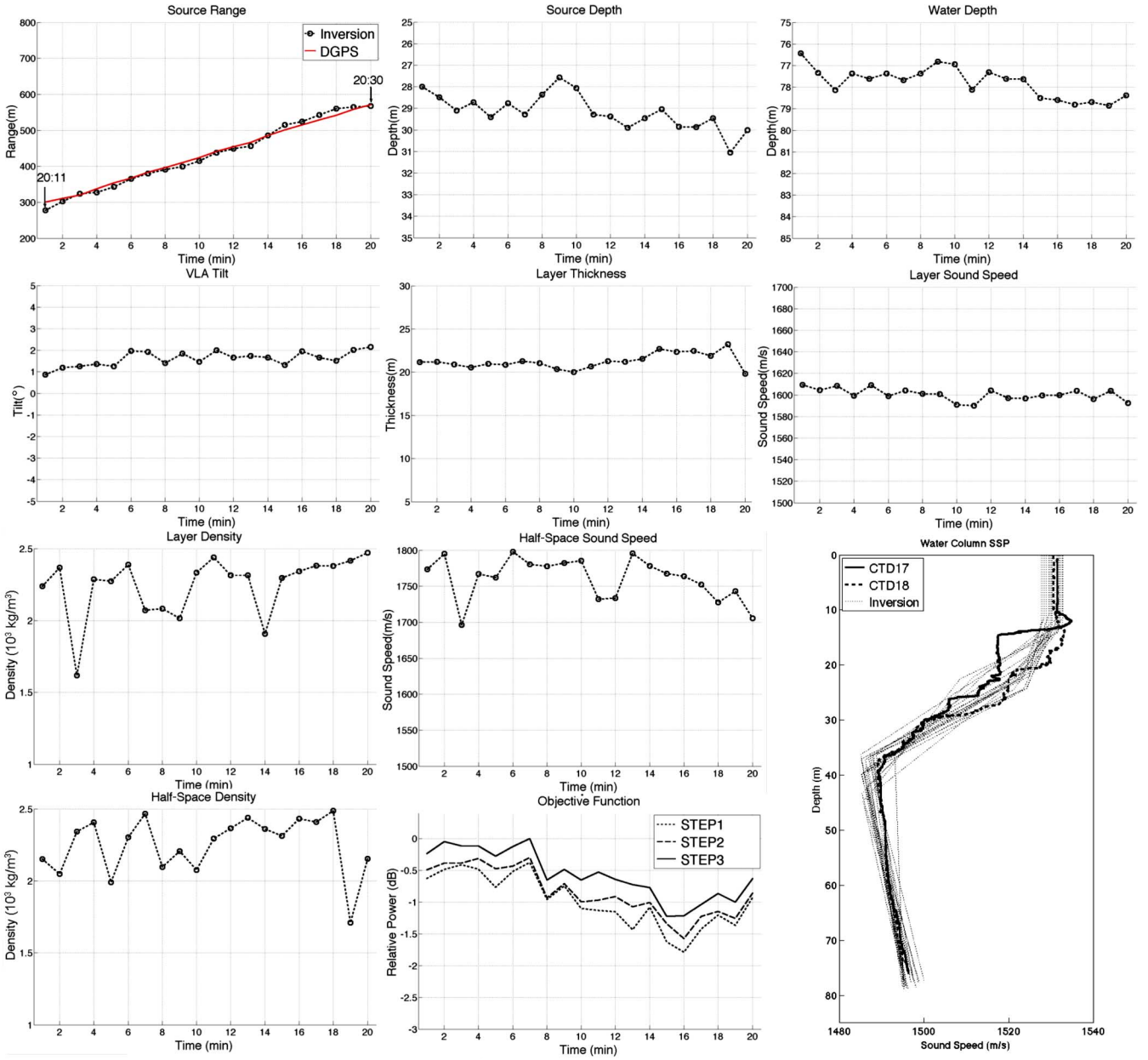

Fig. 10. Inversion results from the straight event (20:11:00 to 20:30:00 UTC). In the plot of source range, the range estimated from the ship DGPS is compared with the inverted range.

data received at a hydrophone consist of coherent signals from distinct eigenray paths. The impulse response is a function of the amplitudes and the phases of their paths. The phase is determined both by the travel times of the eigenrays and by complex reflection coefficients.

At first, a ray is assumed to be emanating from the source with incident angle through a medium with a linear SSP such as

$$c(z) = c(z_1) + a(z - z_1), \quad z_1 \le z \le z_2 \tag{A1}$$

where $c(z_1)$ is the sound speed at a depth of z_1 and a is the constant gradient of the SSP. According to Snell's law, the travel length and the travel time between a start point z_i and an end point z_f become

$$L_{i\_f} = \frac{c(z_i)}{a\sin(\theta_i)}(\cos(\theta_i) - \cos(\theta_f)) \tag{A2}$$

$$t_{i\_f} = \frac{1}{a}\log_e \frac{(z_f - z_1 + c(z_1)/a)(1+\cos(\theta_i))}{(z_i - z_1 + c(z_1)/a)(1+\cos(\theta_f))}. \tag{A3}$$

If the gradient a is zero, i.e., constant sound speed, the ray paths become straight. Then, (A2) and (A3) are not applicable but calculations of travel time and travel length are straightforward from the coordinates of the points and the constant sound speed.

When the ray reaches an interface, call it a branch point, it reflects and transmits with changes in both the propagation angles and amplitudes. If we ignore geometrical spreading for the time being and assume a planar interface, the angles and the amplitudes are easily calculated. The branch points are tracked and stored until the ray reaches the receiver range. The ray is determined as an eigenray if it arrives at the receiver position within a predetermined error bound. Considering geometrical spreading

loss, the complex amplitude of the eigenray having N_b branch points is calculated by

$$A_{\text{eigen}}(f) = \frac{1}{L_{\text{tot}}} \prod_{i=1}^{N_b} A^i_{\text{branch}} \exp\left(-\frac{\alpha_i}{40\pi \log e} k_i(f) L^i_{\text{branch}} \right) \tag{A4}$$

where L_{tot} and L^i_{branch} are travel lengths from the source to the receiver and between adjacent branch points, respectively. A^i_{branch} is the reflection or transmission coefficient depending on the propagation pattern of the eigenray. In addition, $\alpha_i(dB/\lambda)$ is the attenuation coefficient and $k_i(f)$ is the wave number for a frequency f. Finally, the discrete impulse response for all N_e eigenrays becomes

$$h(t) = \frac{\text{Re}\left(\int_{f_1}^{f_2} \sum_{i=1}^{N_e} A^i_{\text{eigen}}(f) \exp\left(i2\pi f \left(t - \tau^i_{\text{tot}}\right)\right) df \right)}{(f_2 - f_1)} \tag{A5}$$

where τ_{tot} is a travel time between the source and the receiver and f_1 and f_2 are the minimum and maximum frequencies of the broadband source, respectively. Removing the frequency dependence of (A4) by approximating the wave number as that at the center frequency, (A5) can be calculated as

$$h(t) = \sum_{i=1}^{N_e} \frac{\left|A^i_{\text{eigen}}\right|}{f_2 - f_1} \left[\frac{\sin\left(2\pi f_2 \left(\tau^i_{\text{tot}} - t\right) + \phi_i\right)}{\pi\left(\tau^i_{\text{tot}} - t\right)} - \frac{\sin\left(2\pi f_1 (\tau^i_{\text{tot}} - t) + \phi_i\right)}{\pi\left(\tau^i_{\text{tot}} - t\right)} \right] \tag{A6}$$

where $\left|A^i_{\text{eigen}}\right|$ and ϕ_i represent the amplitude and phase of A^i_{eigen}.

REFERENCES

[1] C. F. Mecklenbräuker and P. Gerstoft, "Objective functions for ocean acoustic inversion derived by likelihood methods," *J. Comput. Acoust.*, vol. 48, no. 2, pp. 259–270, 2000.

[2] J.-P. Hermand and P. Gerstoft, "Inversion of broadband multitonal acoustic data from the yellow shark summer experiments," *IEEE J. Ocean. Eng.*, vol. 21, no. 4, pp. 324–346, Oct. 1996.

[3] J.-P. Hermand, "Broad-band geoacoustic inversion in shallow water from waveguide impulse response measurements on a single hydrophone: Theory and experimental results," *IEEE J. Ocean. Eng.*, vol. 24, no. 1, pp. 41–66, Jan. 1999.

[4] L. Jaschke and N. R. Chapman, "Matched field inversion of broadband data using the freeze bath method," *J. Acoust. Soc. Amer.*, vol. 106, no. 4, pp. 1838–1851, 1999.

[5] Z.-H. Michalopoulou, "Matched-impulse-response processing for shallow-water localization and geoacoustic inversion," *J. Acoust. Soc. Amer.*, vol. 108, no. 5, pp. 2082–2090, 2000.

[6] P. Pignot and N. R. Chapman, "Tomographic inversion of geoacoustic properties in a range-dependent shallow-water environment," *J. Acoust. Soc. Amer.*, vol. 110, no. 3, pp. 1338–1348, 2001.

[7] C. Park, W. Seong, P. Gerstoft, and M. Siderius, "Time domain geoacoustic inversion of high-frequency chirp signal from a simple towed system," *IEEE J. Ocean. Eng.*, vol. 28, no. 3, pp. 468–478, Jul. 2003.

[8] C. Park, W. Seong, and P. Gerstoft, "Geoacoustic inversion in time domain using ship of opportunity noise recorded on a horizontal towed array," *J. Acoust. Soc. Amer.*, vol. 117, no. 4, pp. 1933–1941, 2005.

[9] Y.-M. Jiang, N. R. Chapman, and P. Gerstoft, "Short range geoacoustic inversion with vertical line array," *J. Acoust. Soc. Amer.*, vol. 124, no. 3, pt. 2 of 2, pp. EL135–EL140, 2008.

[10] C. S. Clay, "Optimum time domain signal transmission and source localization in a waveguide," *J. Acoust. Soc. Amer.*, vol. 81, no. 3, pp. 660–664, 1987.

[11] A. Parvulescu and C. S. Clay, "Reproducibility of signal transmission in the ocean," *Radio Electron. Eng.*, vol. 29, pp. 223–228, 1965.

[12] R. K. Brienzo and W. S. Hodgkiss, "Broadband matched-field processing," *J. Acoust. Soc. Amer.*, vol. 94, no. 5, pp. 2821–2831, 1993.

[13] D. J. Tang, J. Moum, J. Lynch, P. Abbot, R. Chapman, P. Dahl, T. Duda, G. Gawarkiewicz, S. Glenn, J. Goff, H. Graber, J. Kemp, A. Maffei, J. Nash, and A. Newhall, "Shallow Water '06—A joint acoustic propagation/nonlinear internal wave physics experiment," *Oceanography*, vol. 20, no. 4, pp. 156–167, 2007.

[14] T. A. Davies, J. A. Austin, Jr., M. B. Lagoe, and D. Milliman, "Late quaternary sedimentation off New Jersey: New results using 3-D seismic profiles and cores," *Mar. Geol.*, vol. 108, pp. 323–343, 1992.

[15] A. Turgut, D. Lavoie, D. J. Walter, and W. B. Sawyer, "Measurements of bottom variability during SWAT New Jersey Shelf Experiments," in *Impact of Littoral Environmental Variability on Acoustic Predictions and Sonar Performance*. Norwell, MA: Kluwer, 2002, pp. 91–98.

[16] J. A. Goff, B. J. Kraft, L. A. Mayer, S. G. Schock, C. K. Sommerfield, H. C. Olson, S. P. S. Gulick, and S. Nordfjord, "Seabed characterization on the New Jersey middle and outer shelf: Correlatability and spatial variability of seafloor sediment properties," *Mar. Geol.*, vol. 209, pp. 147–172, 2004.

[17] Y.-M. Jiang, N. R. Chapman, and M. Badiey, "Quantifying the uncertainty of geoacoustic parameter estimates for the New Jersey shelf by inverting air gun data," *J. Acoust. Soc. Amer.*, vol. 121, no. 4, pp. 1879–1894, 2007.

[18] J. W. Choi, P. H. Dahl, and J. A. Goff, "Observations of the R reflector and sediment interface reflection at the Shallow Water '06 central site," *J. Acoust. Soc. Amer.*, vol. 124, pp. EL128–EL134, 2008.

[19] O. Coutant, J. Virieux, and A. Zollo, "Numerical source implementation in a 2D finite difference scheme for wave propagation," *Bull. Seismol. Soc. Amer.*, vol. 85, no. 5, pp. 1507–1512, 1995.

[20] Y. Zeng and Q. Liu, "A staggered-grid finite-difference method with perfectly matched layers for poroelastic wave equations," *J. Acoust. Soc. Amer.*, vol. 109, no. 6, pp. 2571–2580, 2001.

[21] S. Kim, G. F. Edelmann, W. A. Kuperman, W. S. Hodgkiss, and H. C. Song, "Spatial resolution of time-reversal arrays in shallow water," *J. Acoust. Soc. Amer.*, vol. 110, no. 2, pp. 820–829, 2001.

[22] C. F. Huang, P. Gerstoft, and W. S. Hodgkiss, "Effect of ocean sound speed uncertainty on matched-field geoacoustic inversion," *J. Acoust. Soc. Amer.*, vol. 123, pp. EL162–EL168, 2008.

[23] P. Ratilal, P. Gerstoft, and J. T. Goh, "Subspace approach to inversion by genetic algorithms involving multiple frequencies," *J. Comput. Acoust.*, vol. 6, pp. 99–115, 1998.

[24] L. Ingber, "Very fast simulated reannealing," *Math. Comput. Model.*, vol. 12, no. 8, pp. 967–993, 1989.

[25] M. K. Sen and P. L. Stoffa, *Global Optimization Methods in Geophysical Inversion*. Amsterdam, The Netherlands: Elsevier, 1995, ch. 4.

[26] P. Gerstoft and D. F. Gingras, "Parameter estimation using multifrequency range-dependent acoustic data in shallow water," *J. Acoust. Soc. Amer.*, vol. 99, no. 5, pp. 2839–2850, 2007.

Cheolsoo Park received the B.S., M.S., Ph.D. degrees in naval architecture and ocean engineering in 1997, 1999, and 2003, respectively, from Seoul National University, Seoul, Korea.

In 2002, he was a visiting student at Marine Physical Laboratory, University of California, San Diego. From 2003 to 2004, he worked at Seoul National University as a Postdoctoral Researcher on Geoacoustic Inversions. In 2009, he was a visiting scholar at Marine Physical Laboratory, Scripps Institution of Oceanography, University of California San Diego (UCSD), La Jolla. Currently, he is a Senior Researcher at Korea Ocean Research and Development Institute (KORDI), Daejeon, Korea. His main research interests are in geoacoustic inversion, ship radiated noise experiment using a large cavitation tunnel, and structural health monitoring.

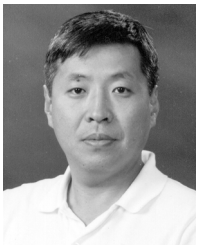

Woojae Seong (M'01) was born in Seoul, Korea. He received the B.S. and M.S. degrees in naval architecture and ocean engineering from Seoul National University, Seoul, Korea, in 1982 and 1984, respectively, and the Ph.D. degree in ocean engineering from Massachusetts Institute of Technology, Cambridge, in 1991.

From 1992 to 1996, he was an Associate Professor at Inha University, Inchon, Korea. Since 1996, he has been a member of the faculty of the Department of Ocean Engineering, Seoul National University, Seoul, Korea. In 2002–2003, he was a Visiting Scientist at Marine Physical Laboratory, Scripps Institution of Oceanography, University of California San Diego (UCSD), La Jolla, where currently he is a Visiting Scientist for the second time (2009–2010). His current research interests are in acoustic propagation modeling in realistic ocean environments with emphasis on treating the bottom as a porous medium, reverberation modeling, geoacoustic inversions, and matched field processing.

Prof. Seong is an associate member of the National Academy of Engineering of Korea.

Peter Gerstoft received the M.Sc. degree from the University of Western Ontario (in the Alan G Davenport Wind Engineering Group), London, ON, Canada, in 1984 and the M.Sc. and the Ph.D. degrees in structural engineering from the Technical University of Denmark, Lyngby, Denmark, in 1983 and 1986, respectively.

From 1987 to 1992, he was employed at Ødegaard and Danneskiold-Samsøe, Copenhagen, Denmark, working on forward modeling and inversion for seismic exploration, and from 1989 to 1990, he was a Visiting Scientist at the Ocean Engineering Department, Massachusetts Institute of Technology, Cambridge, and at Woods Hole Oceanographic Institution, Woods Hole, MA. From 1992 to 1997, he was a Senior Scientist at SACLANT Undersea Research Centre, La Spezia, Italy, where he developed the SAGA inversion code, which is used for ocean acoustic and electromagnetic signals. Since 1997, he has been with Marine Physical Laboratory, Scripps Institution of Oceanography, University of California San Diego (UCSD), La Jolla. His research interests include global optimization, modeling and inversion of acoustic, elastic, and electromagnetic signals.

Dr. Gerstoft is a Fellow of the Acoustical Society of America and elected member of the International Union of Radio Science, Commission F.

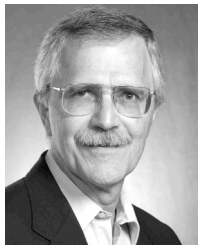

William S. Hodgkiss (S'68–M'75) received the B.S.E.E. degree from Bucknell University, Lewisburg, PA, in 1972, and the M.S. and Ph.D. degrees in electrical engineering from Duke University, Durham, NC, in 1973 and 1975, respectively.

From 1975 to 1977, he worked with the Naval Ocean Systems Center, San Diego, CA. From 1977 to 1978, he was a faculty member at the Electrical Engineering Department, Bucknell University. Since 1978, he has been a member of the faculty of the Scripps Institution of Oceanography, University of California San Diego (UCSD), La Jolla, and on the staff of the Marine Physical Laboratory where currently he is Deputy Director. During 1998–2002, he served as Deputy Director—Scientific Affairs for the Scripps Institution of Oceanography. Currently, he also serves as Associate Director for the UCSD Division of the California Institute for Telecommunications and Information Technology (Calit2). His present research interests are in the areas of signal processing, communications, propagation modeling, environmental inversions, and wireless sensor networks, with applications of these to underwater acoustics and electromagnetic wave propagation.

Dr. Hodgkiss is a Fellow of the Acoustical Society of America.